JOHNSON MATTHEY
TECHNOLOGY REVIEW

www.technology.matthey.com

Johnson Matthey's international journal of research exploring science and technology in industrial applications

**********Accepted Manuscript**********

This article is an accepted manuscript

It has been peer reviewed and accepted for publication but has not yet been copyedited, house styled, proofread or typeset. The final published version may contain differences as a result of the above procedures

It will be published in the **APRIL 2021** issue of the *Johnson Matthey Technology Review*

Please visit the website https://www.technology.matthey.com/ for Open Access to the article and the full issue once published

Johnson Matthey Technology Review
Johnson Matthey Plc
Orchard Road
Royston
SG8 5HE
UK
Tel +44 (0)1763 253 000
Email tech.review@matthey.com

State-of-the-art iridium-based catalysts for acidic water electrolysis: a minireview of wet-chemistry synthesis methods

Himanshi Dhawan,[a] Prof. Marc Secanell,[b] Prof. Natalia Semagina[a,*]

[a] *Department of Chemical and Materials Engineering, University of Alberta, Edmonton, Alberta T6G 2V4, Canada;* [b] *Department of Mechanical Engineering, University of Alberta, Edmonton, Alberta T6G 2V4, Canada.* * Corresponding author: semagina@ualberta.ca

Abstract

With the increasing demand for clean hydrogen production, both as a fuel and an indispensable reagent for chemical industries, acidic water electrolysis has attracted considerable attention in academic and industrial research. Iridium is a well-accepted active and corrosion-resistant component of catalysts for oxygen evolution reaction (OER). However, its scarcity demands breakthroughs in catalyst preparation technologies to ensure its most efficient utilization. This minireview focusses on the wet-chemistry synthetic methods of the most active and (potentially) durable Ir catalysts for acidic OER, selected from the recent publications in the open literature. The catalysts are classified by their synthesis methods, with authors' opinion on their practicality. The review may also guide the selection of the state-of-the-art Ir catalysts for benchmarking purposes.

Graphical Abstract

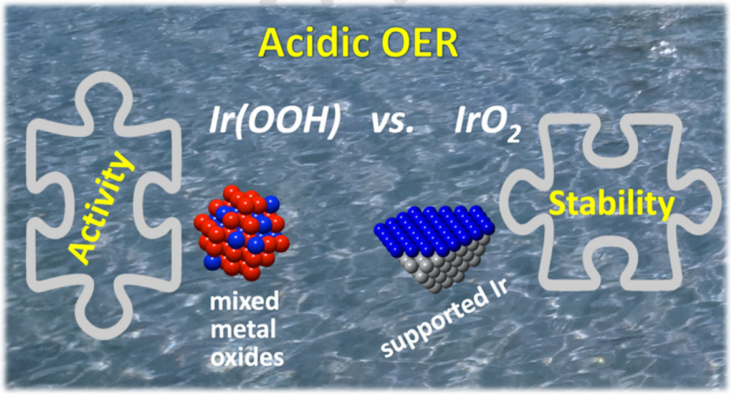

Abbreviations

ATO: Antimony tin oxide
BET: Brunauer–Emmett–Teller
CCM: Catalyst coated membrane
CTAB: Cetyltrimethylammonium bromide
ECSA: Electrochemically active surface area
FTO: Fluorine tin oxide
GCN: Graphitic carbon nitride
GHG: Greenhouse gas
ITO: Indium tin oxide
NSTF: Nanostructured thin film
OER: Oxygen evolution reaction
PEM: Proton exchange membrane
PTL: Porous transport layer
TaTO: Tantalum tin oxide
TOF: Turnover frequency
TTAB: Tetradecyltrimethylammonium bromide
UC: Umicore

Doi: 10.1595/205651321X16013966874707

1. Introduction

Hydrogenations and hydrotreating reactions with molecular H_2 are critical operations in chemical and related industries. Regardless of the nature of the hydrotreated reactants and products, as society walks away from fossil fuels, the need for hydrogen will remain indispensable. With the increasing access to surplus renewable electricity, the H_2 production by water electrolysis may take its rightful place not only in transportation and energy storage, but also as a clean H_2 supply for chemical and related industries,(1) replacing GHG-producing methane steam reforming. Among the commercialized and emerging technologies, acidic PEM electrolyzers can operate at up to 20 A/cm^2 current density and deliver up to 700 bar H_2 at high efficiencies.(2) Active and durable electrocatalysts are required to reduce the power input, the bottleneck being the sluggish anodic OER. The acidic environment, however, demands corrosion-resistant materials at high potentials. The winner so far is the OER-active conductive and corrosion-resistant iridium at typical loadings of 1-2 mg/cm^2. Lower Ir requirements were demonstrated, for example, for a PEM electrolyzer with the 3M NSTF catalyst reaching 2 A/cm^2 current density at 1.86 V at 0.25 mg$_{Ir}$/cm^2,(3) which translates into ca. 100 tonnes Ir for the production of 1 TW H_2.(4) It is obvious that with the current technologies, the terawatt-scale hydrogen production cannot be met with the annual supply of scarce Ir of less than 10 tonnes.(4) The annual global demand of hydrogen was reported as 73.9 Mt$_{H2}$ in 2018; as it is almost entirely supplied from fossil fuels, its current production emits 830 Mt of CO_2 per year.(5) The H_2 production replacement in chemical industries with water electrolysis is relatively well-positioned as a target area for decarbonization of the industrial sector.

Hundreds of research papers have been focussed on the development of active and durable Ir catalysts, deposition techniques, and associated catalyst layer components, which may limit the performance of the most active Ir catalyst formulations. Recent reviews classified Ir-containing catalysts for acidic OER (6) and the variety of methods for the synthesis of iridium oxide (7). Commercial catalyst production methods must be scalable, preferably not require specialized equipment apart from what is available in the catalyst production industries, not produce significant waste, and lack the need for large amounts of chemicals, especially those that are hazardous to the environment. With this in mind, the objective of the current minireview is to select a number of the most efficient state-of-the-art Ir catalysts for acidic OER within reported wet-chemistry synthesis methods, focussing on the practicality and scalability of the techniques. We address only wet-chemistry routes, as they are most

Doi: 10.1595/205651321X16013966874707

frequently reported, being relatively accessible in a research environment. Fig. 1 and Table 1 summarize the catalyst synthetic routes and selected catalysts, addressed in this review; this is not a comprehensive summary of all possible routes and catalysts, but rather a careful selection of studies demonstrating promising combination of activity and stability in acidic OER.

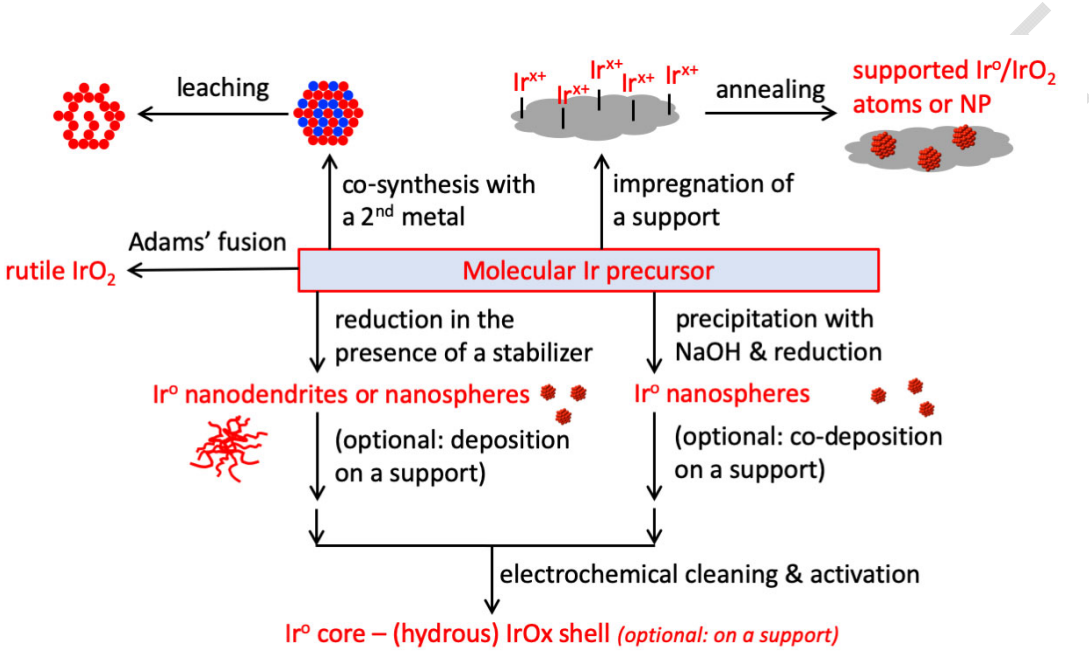

Figure 1. Summary of the reviewed wet-chemistry synthetic routes of state-of-the-art Ir catalysts for acidic OER

The catalyst layer preparation methods, such as deposition methods, are out of the scope of this work, although they significantly affect the catalyst performance. Gas-phase catalyst (layer) preparation techniques (8, 9) are omitted for the same reason, as they require specialized equipment and feature simultaneous catalyst formation and its deposition. The review is based only on published research works; we acknowledge that it may become obsolete due to the rapid developments in the field, or may miss some critical proprietary information. The citations are chosen only to support our viewpoints; they cannot be considered as a comprehensive list of the relevant works. Herein, we aim to provide comprehensive insights in selected promising wet-synthesis methods. We hope that the review may help the reader in the selection of a state-of-art catalyst for benchmarking purposes, as well as to assist in further developments of potentially scalable synthesis of active and durable Ir catalysts.

Doi: 10.1595/205651321X16013966874707

*Table 1. Summary of the state-of-the-art activities of selected catalysts prepared by wet-chemistry synthesis and tested in an RDE**

Catalyst (method) and section *vide infra*	Loading on the electrode, mg_{Ir}/cm^2	Overpotential at 10 mA/cm^2, mV	Activity	Ref.
3.2. Surfactant-assisted	0.061	~ 290	100 A/g_{Ir} at 1.51 V_{RHE}	(10)
3.3 Surfactant-free colloids	0.0071	345	205 A/g_{Ir} at 1.5 V_{RHE}	(11)
4. Supported on GCN	0.07	278	580 A/g_{Ir} at 1.55 V_{RHE}	(12)
4. Supported on TaTO	0.02	~ 300	250 A/g_{Ir} at 1.51 V_{RHE}	(13)
5.2. Selective leaching	0.0277	N/A	810 A/g_{Ir} at 1.51 V_{RHE} 3353 A/g_{Ir} at 1.55 V_{RHE}	(14)

* Note that the data are mostly reported for the fresh catalysts. Stability data, where available, are discussed in the text.

2. Requirements to the iridium catalyst performance and structure: activity vs. stability

Bernt (15, 16) estimated that, in order to decarbonize the transportation sector by transitioning to fuel cell vehicles fuelled by renewable hydrogen, the metal loadings on the anode of polymer electrolyte water electrolyzers should be decreased to 0.05 mg_{Ir}/cm^2. This loading can meet the demand for approximately 150 GW/year installed capacity while using only 50% of the annual Ir production. In order to meet this requirement and also use electrolysis for other needs, such as energy storage and chemical industry supply, the specific Ir activity must be increased substantially. An ideal OER catalyst would have negligible overpotential; a highly desirable catalyst would be one that requires 200-300 mV overpotential (1.43-1.53 V) at 10 mA/cm^2 current, with catalysts achieving this same current density at overpotentials of 300-400 mV (1.53-1.63 V) being acceptable.(17) As a durability criterion, if the overpotential is maintained for 10 h, the catalyst may be suitable for real device fabrication, taking into consideration the catalyst nature and mass loading as well.(17) The high activity would manifest itself in a low Tafel slope at real operating potentials. The

Doi: 10.1595/205651321X16013966874707

catalyst specific activity (specific current for electrocatalysis) is the product of the following catalyst characteristics, assuming ideal kinetics with no transport limitations:

*Specific activity [A/g_{Ir}] = Intrinsic activity (TOF) [A/$mol_{active\ sites}$] * Active/surface site stoichiometrty [$mol_{active\ sites}$/$mol_{surface\ atoms}$] * Ir dispersion [$mol_{surface\ atoms}$/$mol_{Ir\ total}$] / 192 [g_{Ir}/mol_{Ir}]*

This equation clarifies that it is not enough to develop highly dispersed Ir catalysts, which would be a relatively easy task to do by synthesizing sub-2 nm Ir particles with >50% dispersion but that a proper type of Ir species must dominate the surface. Furthermore, the involved parameters must be stable over the device lifetime.

The activity of the catalyst is usually dependant on the OER pathway, which has been shown to depend on the treatment of the Ir catalyst. In general, two mechanisms have been proposed, with the main difference being the predominant involvement of electron-deficient electrophilic oxygen (denoted as O^{I-}) and/or as activated lattice oxygen in the reaction. The OER on rutile-type IrO_2 proceeds by means of the classical oxide, electrochemical oxide, or electrochemical peroxide pathways involving M-O, M-OH and M-OOH intermediates (18, 19):

(1) $M + H_2O \rightarrow M\text{-}OH_{ads} + H^+ + e^-$

(2, oxide) $2M\text{-}OH_{ads} \rightarrow M\text{-}O_{ads} + M + H_2O$

(2, electrochemical and peroxide) $M\text{-}OH_{ads} \rightarrow M\text{-}O_{ads} + H^+ + e^-$

(3) $2M\text{-}O_{ads} \rightarrow 2M + O_2$

(3, peroxide) $M\text{-}O_{ads} + H_2O \rightarrow M\text{-}OOH_{ads} + H^+ + e^-$

(4, peroxide) $M\text{-}OOH_{ads} \rightarrow M + O_2 + H^+ + e^-$,

where M represents the metal oxide IrO_2.The peroxide pathway has recently been shown to provide trends that are in agreement with experimental observations by Schuler et al. (19) The electrochemical oxide path is highlighted in red in Fig. 2.

Catalyst featuring an electrochemically grown porous hydrous oxide layer, also known as oxy-hydroxide layer or amorphous IrO_x catalysts, exhibit an OER mechanism that involves an electrophilic O^{I-} species (20) and/or an activated lattice oxygen pathway.(21, 22) According to Geiger et al. (21), a simplified pathway highlighting the need for the outer layer of the catalyst to be involved in the reaction could be:

(1) $Ir\text{-}x\text{-}Ir + H_2O \rightarrow Ir\text{-}O\text{-}Ir + 2H^+ + 2e^-$

(2) $Ir\text{-}O\text{-}Ir + H_2O \rightarrow IrO_2 + 2H^+ + 2e^-$

Doi: 10.1595/205651321X16013966874707

(3) $IrO_2 \rightarrow Ir\text{-}x\text{-}Ir + O_2$

where "x" is a vacancy in the porous hydrous oxide layer. Other references have attributed the increased activity to electrophilic O^{I-} species. (20) Ir-O-Ir would play a similar role to the proposed highly reactive, electrophilic oxygen O^{I-} species.(20, 23) The second step would have a similar function to the preliminary reaction proposed by Pfeifer et al., i.e., $IrO_xO + H_2O \rightarrow IrO_x\text{-}O\text{-}O\text{-}H + H^+ + e^-$, (23) where IrO_xO represents the iridium oxide matrix with an adsorbed oxygen. The pathway involving the electrophilic O^{I-} species is also highlighted in Fig. 2 in green, where $HIrO_2$ would loosely represent the O^{I-} intermediate.

The OER has been shown to be more active for the pathway involving the electrophilic O^{I-} species and/or activated lattice oxygen. Unfortunately, this pathway tends to be deactivated due to the lattice oxygen evolution leading to iridium dissolution, and to the transformation of the oxo-hydroxide to less active anhydrous species. (21, 24–26) Stabilization of the iridium atoms in the pathway involving the electrophilic O^{I-} intermediate via enhanced crystallinity (25) or the use of mixed oxides could minimize stability issues. Crystalline IrO_2 has a lower intrinsic activity but is more stable due to strong Ir-O bonds between IrO_6 clusters, with only topmost layers of the rutile contributing to both processes.(24) The superior stability of thermal iridium oxide is explained by slower kinetics of IrO_3 hydrolysis as compared to its decomposition.(27) It has been suggested that both pathways occur during the OER with the activated lattice oxygen pathway being dominant at low potential, due to its high activity, and the classical pathway being dominant at higher potential.(27) At potentials relevant to the OER, it is possible that the oxo-hydroxide layer slowly transforms to anhydrous oxide with a subsequent loss in activity and enhancement in stability as recently shown by atomic probe tomography.(26)

Doi: 10.1595/205651321X16013966874707

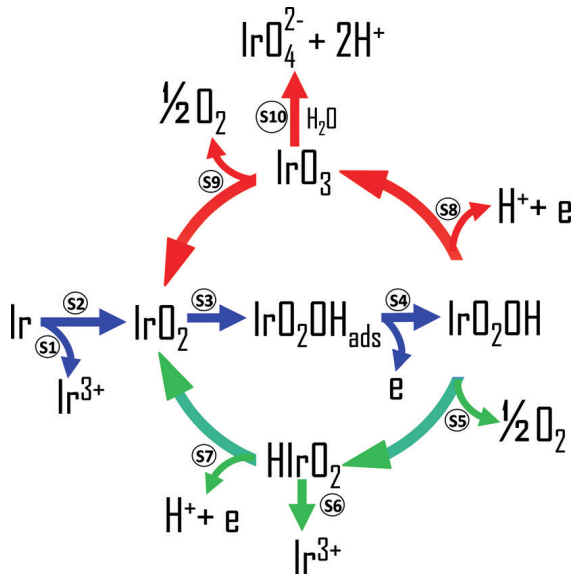

Figure 2. OER (green arrows) and deactivation (red arrows) pathways in acidic OER, with green route being preferable at lower potentials, red route at higher potentials, while the blue route is potential independent. Reprinted with permission from (27)*, copyright John Wiley and Sons 2018.*

Speaking of which Ir phase is to be synthesized and introduced into the electrochemical device, the literature features metallic Ir with a variety of predominant crystallographic orientations, amorphous hydrous iridium oxide, crystalline rutile IrO_2, their mixtures, as well as multimetallic Ir composites. The metallic Ir may be oxidized by calcination in air before the catalyst layer assembly (28) or electrochemically *in situ*. (25, 29) Thermal iridium oxidation to IrO_2 occurs between 200 and 500 °C, (30) the higher the temperature, the higher the crystallinity and electrochemical stability, but the surface area and the activity decrease.(31) The 400 – 500 °C region was recommended to strike a balance between activity, stability and conductivity.(28)

Many state-of-the-art catalysts, as shown below, use electrochemical *in situ* oxidation. The Ir (110) surface evolves into two chemically different Ir species, with an active accessible oxide-metal interface. (32) The most dense (111) Ir surface is more resistant to the oxidation, and once the oxide is formed, the metallic interface is buried. Although the kinetics of oxide formation and redox properties of the two surfaces are different, their final reached OER activities are rather similar. The same work (32) recommends that for the formation of a porous hydrous IrO_2, the *in situ* Ir(0) activation should include oxidizing-reducing cycles,

Doi: 10.1595/205651321X16013966874707

instead of conventionally used electrooxidation, although another study argues that the repetitive electrochemical oxidation/reduction unavoidably leads to dissolution.(33) The electrochemical oxidation proceeds via hydroxide to the irreversible Ir(IV) oxide formation in the nanoparticles, while bulk Ir preserves its metallic subsurface with porous Ir(IV) surface layers.(34) Thus, one must be mindful of the iridium dissolution during electrochemical oxidation via hydrous iridium oxide growth.(33) When 20-nm Ir films are used for the acidic OER, their lifetime is similar to the lifetime of the hydrous iridium oxide and is significantly lower than for crystalline IrO_2.(21)

To produce highly crystalline IrO_2, which is more stable but less active than hydrous iridium oxide, preliminary annealing in air may be recommended, whenever possible. The exceptions, of course, include unsupported polymer-stabilized nanoparticles,(25) where annealing would result in particle agglomeration, as well as metal carbides, where it would lead to oxidation and loss of conductivity.(35) In such cases, the electrochemical oxidation procedure must be optimized as it affects the catalyst stability.

Fine tuning of the oxide crystallinity, crystallographic orientation, number of oxygen defects, and length and strength of Ir-Ir and Ir-O bonds via thoughtful synthetic approaches may diminish the gap between the active but unstable and stable but less active phases. Some such examples, leading to state-of-the-art catalysts, are given below.

Thus, the treasure hunt for the most efficient Ir OER catalyst is a simultaneous optimization of activity vs. stability. In addition, in order to achieve high Ir utilization, the catalyst must be easy to integrate into a catalyst layer in order to yield a layer than has both low loadings, and excellent charge and mass transport. Charge transport should include both electronic and protonic in-plane and through-plane conductivities. Proton transport can be optimized by controlling the amount of electrolyte in the layer,(36, 37) while improving electron conductivity can be achieved with the use of a conductive support and interconnected IrO_x network. Similarly, good in-plane conductivity could be maximized by using a PTL with a microporous layer. (38)

The catalyst lifetime depends on its operating current density and overpotential. It may be estimated using the so-called activity-stability factor (39) or stability number S, (21) i.e., the ratio of evolved oxygen to dissolved Ir at constant overpotential (39). Geiger et al. reported that IrO_2 powder features a 1-year lifetime at 200 A/g_{Ir} vs. 1 month for hydrous oxide.(21)

Doi: 10.1595/205651321X16013966874707

The numbers are specific to the used electrochemical cell (Fig. 3); for example, oxygen bubble accumulation, a common occurrence in RDE, could make the stability studies not a reliable predictor for the catalyst lifetime in a PEM electrolyzer long-term behavior.(16) In a PEM electrolyzer, iridium dissolution might result in both iridium ions in the water feed, and migration and redeposition at the anode/membrane interface, membrane,(40–42) and possible deposition on the cathode leading to Pt deactivation, especially at high current densities and overpotentials.(42)

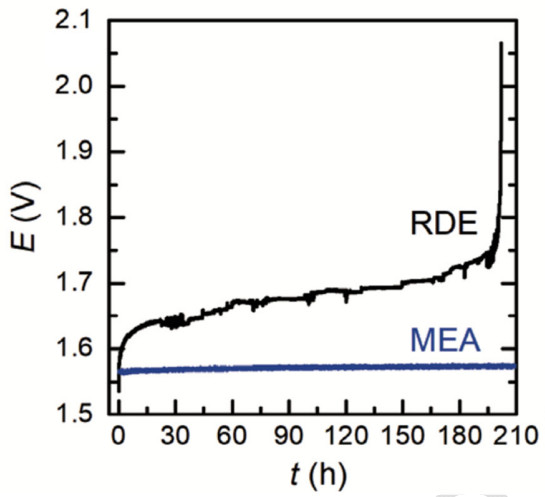

Figure 3. Evaluation of IrO_2/TiO_2 catalyst stability in an RDE and MEA at 70 A/g_{Ir}; reprinted from (16) *under the Creative Commons Attribution License, copyright 2019 The Authors.*

Last but not least, even if the most ideal active and stable Ir phase is developed, the benefits will only manifest itself if other occurring phenomena are not rate-limiting. The high intrinsic activity and stability may be masked by the limitations in the characterization technique used, or by the electrode fabrication methodology.(43, 44) For example, the commonly used RDE technique might be subject to inert backing passivation,(44) and catalyst coated membrane (CCM) fabrication techniques, such as spray-coating, doctor blade, and inkjet printing method, could result in very different electrode structures for full-cell testing. Inadequate RDE or CCM fabrication, or non-optimal electrolyte loading can result in excessive charge and mass transport limitations. Further, possible causes of loss of activity are poisoning of the catalyst surface by Nafion,(45) impurities in the electrolyte in RDE. In the presence of non-Ir components, cations place-exchange with sulfonic acid groups in the polymer electrolyte

Doi: 10.1595/205651321X16013966874707

resulting in decreased proton conductivity.(46) All these complicate not only the scale-up, but also the assessment of the intrinsic catalyst performance in lab-scale devices. It is possible that efficient catalysts have not been identified because of these limitations. Some benchmarking procedures for the OER evaluation have been proposed in RDE (25, 47) and alternative liquid-flow (44, 48, 49) or vapor-fed cells,(19) and are urgently needed to be followed.

3. Synthesis of unsupported Ir/IrO_x/Ir-OOH catalysts

3.1. Adams' fusion method

Adams' method was originally developed to conquer the issues of irreproducible platinum catalyst synthesis; it was successfully scaled up and is used industrially for Pt (Adams') catalyst production (50, 51) and thus is well positioned for a potential scalability. It also appears to be one of the most used methods reported for the synthesis of IrO_2 for OER, including supported and multimetallic composites. The method is based on the synthesis of iridium nitrate from an iridium molecular precursor heated in a solid mixture with sodium nitrate, followed by the iridium nitrate high-temperature decomposition to IrO_2. The side products include poisonous nitrous oxides, which release must be appropriately managed. Synthesis parameters include the temperature and duration of the calcination, nature of the iridium precursor, and its fraction in the mixture with $NaNO_3$, all of which affect the crystallinity, oxidation state, and surface area of the produced material and thus, the OER performance. The higher is the calcination temperature, the higher is the crystallinity of the produced oxide. However, the amount of active surface hydrous iridium oxide decreases, as well as the catalyst surface area. Although the increase in the calcination temperature leads to the lower Ir dispersion (larger particle size) and lower turnover frequency due the formation of less active crystalline IrO_2, the latter is more stable towards dissolution. This indicates the existence of the optimal calcination temperature to achieve the activity-selectivity balance for the maximized Ir utilization.(31) Electrical conductivity is also improved with increased crystallinity at annealing.(52) The highest reported surface area of an Ir oxide produced by a modified Adams' method is 350 m^2/g, which was obtained from iridium acetylacetonate and calcined in air at 350 ^oC for 30 min.(31) The oxide consists of nanodisks with surface partially covered by active Ir(OOH), which however retained only 55% of its activity after 500 potential cycles due to mass loss and restructuring. When the original sample was further heated at 400 ^oC for 1 h, the catalyst retained 70% of its activity after 500 potential cycles. Increased

Doi: 10.1595/205651321X16013966874707

calcination temperature, however, led to a decrease in surface area to 250 m^2/g. At the catalyst loading of 0.1 mg_{IrOx}/cm^2, the specific current of 26 A/g_{IrOx} could be achieved at 295 mV overpotential before the stability tests (0.1 M $HClO_4$). For both catalysts, the same activity loss (of 30%) occurred due to the partial oxidation of active sites, but due to the decreased leaching from the 400 °C-treated sample, the latter strikes the balance between the activity and stability.(31) The increase in calcination temperature leads not only to the surface area decrease but also changes the particle morphology to rods with dominating {110} surface terminations.(53)

Among other promising reported modifications of Adams' method, the addition of cysteamine to the iridium precursor solution resulted in the formation of IrO_2 nanoneedles of 2 nm diameter (6-8 layers of (110) plane, Fig. 4) and 30 nm length after 450 °C calcination.(54) Although the needles possessed lower BET surface area than the catalyst formed without cysteamine (141 vs 197 m^2/g), their electrical conductivity was 6-fold higher. An overpotential of 313 mV was required to achieve 10 mA/cm^2 at the catalyst loading of 0.21 mg_{Ir}/cm^2 (1M H_2SO_4, 25 °C) before and after a 2-h durability test. The needles were also tested in a PEM electrolyzer and found more active and stable than the spherical IrO_2 synthesized without cysteamine.(54) Most likely, the less dense and well-connected structure of Ir needles contributed to the improved porosity and electrical conductivity. Thin needles with near-zero sphericity form packed beds with the highest near-100% porosity as opposed to 40% for the spherical particles.

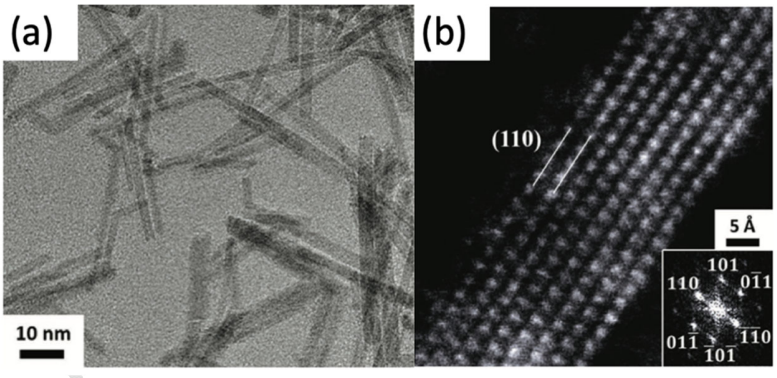

Figure 4. Ultrathin IrO_2 nanoneedles (a) consisting of 8 (110) layers (b). Reproduced from (54) *with permission from John Wiley and Sons. Copyright 2017.*

Doi: 10.1595/205651321X16013966874707

3.2. Iridium nanoparticles stabilized by a capping agent

If one has to produce monodisperse near-spherical nanoparticles with high dispersion (>50%, i.e., smaller than ca. 2 nm) to increase metal utilization or form anisotropic nanostructures to increase the catalyst layer porosity or promote the formation of certain crystal terminations, colloidal synthesis in the presence of a capping agent is a popular method in academic research.(55) Halogen-containing stabilizers, such as CTAB, are known to act also as a growth-directing agent by the halogen selective adsorption on (100) surfaces resulting in rod-like structures. The produced structures are usually pre-washed from the excess chemicals, while the in-situ electrochemical preconditioning removes the surfactant, for example, by 50 potential sweeps from 0.05 to 1.5 V_{RHE}. (29) Since the metallic Ir is oxidized electrochemically, it is likely to possess a higher proportion of activity-relevant hydrous Ir oxide on the surface, as opposed to calcined rutile IrO_2.

One of the most successful examples in this category is the 2.0±0.4 nm Ir nanoparticles formed by $IrCl_3$ reduction in ethanol with excess $NaBH_4$ in the presence of CTAB. (10) $NaBH_4$ is a strong and fast reducing agent to produce metallic nanoparticles and is often used in the colloidal synthesis. In a protic solvent, borohydride decomposes to gaseous hydrogen, which, depending on the conditions, may proceed in a violent manner. To reach 10 mA/cm^2 current, ca. 290 mV overpotential was required at only 0.061 mg_{Ir}/cm^2 loading in an RDE (0.5 M H_2SO_4, 25 °C). The catalyst demonstrated a similar Tafel slope of ca. 40 mV/dec as the calcined catalyst prepared by the Adams' fusion method. (31) However, the specific current at 1.51 V was an order of magnitude higher (100 A/g_{Ir}). The nanoparticles formed a nanoporous structure with well-connected particles, which retained their metallic core but featured an active thin surface oxide layer (Fig. 5a, b). Authors stressed the importance of complete $IrCl_3$ removal by adding excess of reducing agent to prevent inhibition of electron transfer. Although the catalyst showed an order of magnitude higher specific current than Ir black UC in an RDE, it required only 250 mV lower potential to reach 2 A/cm^2 current (1.85 – 1.9 V) when tested in an unoptimized PEM electrolyzer with 1 mg_{Ir}/cm^2 loadings. This again indicates the effect of various factors in a PEM electrolyzer.

Doi: 10.1595/205651321X16013966874707

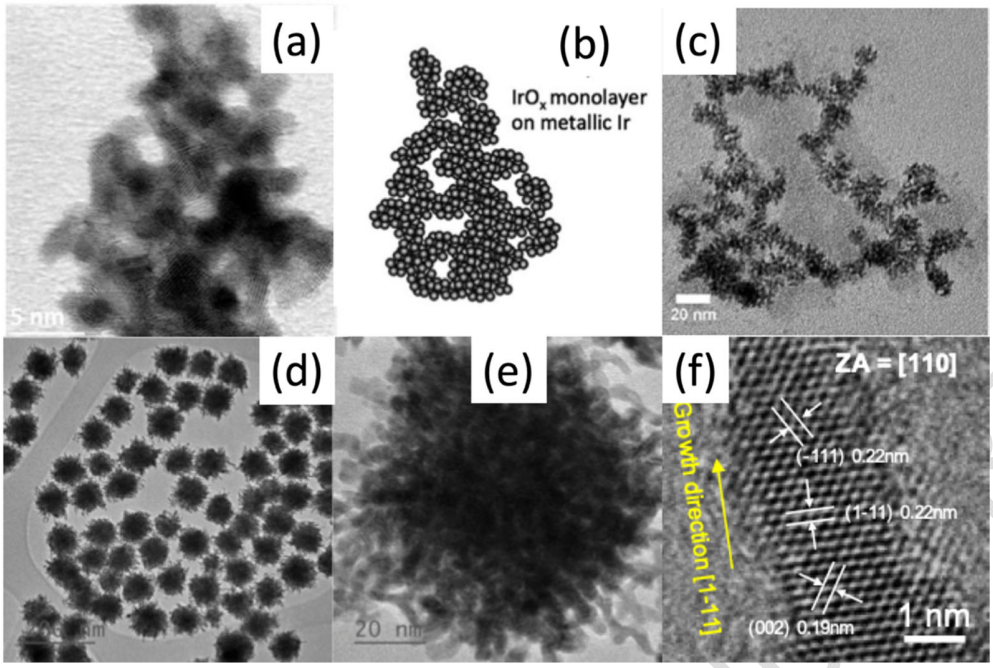

Figure 5. (a, b) Stabilized interconnected Ir nanoparticles (10)*; (c) Ir nanodendrites* (29) *(reproduced from* (10) *and* (29) *under a Creative Commons Attribution 3.0 Unported License, published by The Royal Society of Chemistry); and (d-f) highly-crystalline nanopompons* (25) *(reproduced from* (25) *under a Creative Commons License, published by Elsevier).*

The use of TTAB during IrO_2 precipitation from H_2IrCl_6 by NaOH, followed by reduction by $NaBH_4$, resulted in the formation of 1.7 metallic Ir seeds that self-assembled into nanodendrites with 34% porosity at 39 m^2/g BET surface area.(29) The high crystallinity favored stability toward dissolution. The 10 mA/cm^2 current was achieved at 410 mV overpotential (RDE, 0.05 M H_2SO_4) but at only 0.0102 mg_{Ir}/cm^2 loading. At 1.51 V, the catalyst activity was 70 A/g_{Ir}. Similarly to the CTAB-stabilized particles,(10) the formed structure featured high porosity and well-connected individual particles (Fig. 3c).

When a slow reducing agent is used for synthesis (such as glucose (25)), the CTAB suppressed the grain growth in (100) directions; the nanodendrites self-assembled into nanopompons (Fig. 5d-f). Those highly crystalline structures with a high proportion of low-index crystal terminations were relatively resistant to dissolution but showed lower activity as compared to the hydrous iridium oxide. (25)

Doi: 10.1595/205651321X16013966874707

The stabilizer-assistant synthesis techniques are easy to implement in a wet laboratory without specialized equipment for academic research. This method of Ir synthesis is also used to preform Ir nanostructures prior to their deposition on a support. One must be mindful of a typically low metal concentration in the synthesis solution, the relatively large use of solvents, reductants, stabilizers and washing solutions, many of which are manufactured from fossil resources and expensive. Such synthesis methods are usually too cumbersome for industrial production, the improvements being feasible though for certain stabilizers.(56)

3.3. Stabilizer-free wet chemical synthesis methods

This category features one of the most active catalysts reported to date, although the electrodes were fabricated without Nafion. Synthesis of 1.6±0.3 nm Ir particles was performed without a stabilizer by heating a solution of $IrCl_3$ in methanol, which reduces IrO_2 precipitated by the co-added NaOH; the resulting solution was used without purification. (11, 57) At the loading of 0.0071 mg/cm^2 achieved by drop casting of the native solution, the particles formed a uniform layer on a GC disk. In 0.1 M $HClO_4$, in an RDE, the catalyst demonstrated an outstanding 205 A/g_{Ir} activity at 1.5 V_{RHE} and 1130 A/g_{Ir} at 1.55 V_{RHE}. (57) The ECSA was found to be 140 m^2/g (at the loading of 0.0071 mg_{Ir}/cm^2). The overpotential to reach 10 mA/cm^2 was 345 mV at the 0.0071 mg_{Ir}/cm^2 loading, or 325 mV at the 0.0143 mg_{Ir}/cm^2 loading. (11) The Ir loading on the electrode was of a vital importance: the loading increase above 0.0071 mg/cm^2 resulted in the significant drop of the ECSA and thus specific current. (11) The specific activity at the optimal loading surpasses the activity for the surfactant-mediated catalysts, (10) and features a significantly easier, cheaper and a scalable preparation. In addition to being surfactant-free and using a low-boiling easy recoverable solvent, the method is scalable to high metal concentrations (5 g/L). (57) The fate of Na^+ (10:1 Na:Ir) is to be investigated, as well as the catalyst durability and performance in a PEM electrolyzer.

Many studies feature a similar Ir nanoparticle synthesis without a surfactant with the use of a base (NaOH) in other reducing solvents, but typically such particles are deposited on a support, and are discussed in the Section 4.

Doi: 10.1595/205651321X16013966874707

4. Wet synthesis of Ir catalysts on powdered supports

In heterogeneous catalysis, supports, typically with a high specific surface area, are used to stabilize highly dispersed active metal nanoparticles, both during the catalyst synthesis and to ensure their stability against agglomeration during a reaction. In the case of electrolyzers, the supports can also be used to enhance the electrode electrical conductivity as they will reduce the contact resistance between particles. The acidic OER environment dictates specific requirements to the type of a support: it must be resistant to chemical and electrochemical dissolution, and preferably must have a high electronic conductivity. The latter need is mandatory if Ir loading is low; however, if iridium oxide covers most of the support, it may provide sufficient percolative transport for the electrons.(3) The film, however, must be as thin as possible to provide advantages over unsupported iridium oxide nanoparticles. In this subsection, we focus on the wet synthesis of Ir catalysts on powdered supports, which could be mixed with a Nafion solution for catalyst layer preparation.

In recent years, carbon and metal carbides have been receiving less and less attention because of the carbon oxidation and volatilization to CO_2 at high applied potentials.(58) As a notable exception, one of the most active Ir catalysts reported so far features a carbon-based support.(12) A 40 wt.% Ir catalyst was prepared by impregnation of graphitic carbon nitride (GCN) nanosheets with the metal precursor followed by annealing in air at 350 °C. Thus embedded IrO_2 possesses compressed Ir-Ir bonds and decreased coordination numbers of Ir-O and Ir-Ir, which was suggested to weaken the adsorption of oxygen intermediates leading to increased OER activity. The reported specific currents are 580 A/g_{Ir} at 1.55 V and 1493 A/g_{Ir} at 1.6 V. The catalyst required the overpotential of 278 mV at 10 mA/cm^2 at 0.07 mg_{Ir}/cm^2 loading (in RDE in 0.5 M H_2SO_4). Authors demonstrated only 35 mV potential increase at 20 mA/cm^2 for ca. 4 hours in an RDE; and 78.5% current retention in a laboratory water splitting device after a 24-hour operation at 1.6 V. The fate of GCN was assessed by holding 2.2 V_{RHE} for 2 h with intermediate CV measurements between 0.4 and 0.6 V_{RHE}; the double-layer capacitance decreased by 10% in the first 0.5 h and remained stable up to 2 h (12); apparently, the graphitic support nature with nitrogen heteroatom provides its stability in acidic electrolysis. Given the high catalyst activity and a rather easy and potentially scalable preparation of GCN and Ir/GCN, the studies of the catalyst durability and performance in a PEM electrolyzer are warranted.

Doi: 10.1595/205651321X16013966874707

Among oxidation-resistant conductive metal oxide supports, tin dioxide doped with antimony (ATO), indium (ITO) and fluorine (FTO) have been the focus of the most research because of their relatively high conductivity. Unfortunately, the dopant's corrosion brings down the conductivity, increasing ohmic losses and decreasing the energy efficiency.(59) Dissolved cations may also ion-exchange with the membrane and lead to its degradation. (46) A recent study observed neither activity nor stability benefits from the dopant addition.(60) Although FTO possess the lowest conductivity, it was found to be most stable material between -0.34 V_{RHE} and 2.7 V_{RHE}, followed by ITO and ATO. The stability is assigned to the oxygen atom exchange in SnO_2 with F, instead of cation exchange in case of ATO and ITO synthesis.(59) ATO, in turn, was suggested to mitigate Ir dissolution by preserving it in lower oxidation states.(61) Commercially available samples usually feature low surface areas; several synthetic techniques were suggested in literature for the preparation of mesoporous doped SnO_2 with relatively high areas (for example, between 125 and 263 m^2/g).(62) To deal with toxic NH_4F for the FTO synthesis, safety measures must be in place, as in any chemical and engineering process. A number of Ir catalysts supported on doped SnO_2 with high activities and low overpotentials at low Ir loadings were recently reported.

A popular method for the preparation supported Ir OER catalysts, is a colloidal precipitation of IrO_2 from an iridium molecular precursor by means of NaOH; the synthesis may proceed in ethylene glycol,(29) which serves both as a solvent and a reducing agent, or, for example, in a hydrothermal microwave reactor.(63) Small 2-3 nm particles may be obtained,(61) or even smaller (1.5±0.2 nm) if a stabilizer is added.(64) The support may be added to the colloidal dispersion either during synthesis, or after the nanoparticle formation. The use of high-boiling ethylene glycol, though, complicates the potential process scale-up because solvent removal under vacuum is usually used,(57) instead of centrifugation or filtration of highly diluted suspensions, as practiced in the laboratories. As an example of such preparation method, when SnO_2 was doped with tantalum (TaTO) and used to deposit preformed 1.7 nm IrO_x nanoparticles at 11-18 wt.% Ir loading, the OER activity of the fresh catalysts after electrochemical conditioning approached 250 A/g_{Ir} at overpotentials of 280 mV and 370 mV at 0.020 mg_{Ir}/cm^2 loading (25 ^oC, 0.05 M H_2SO_4).(13) Although the electronic conductivity of TaTO was two orders of magnitude lower than that of ATO, its use did not result in decreased activity, which was ascribed to the conducting role of well dispersed IrO_x nanoparticles. In accelerated ageing tests at 1.2-1.6 V potential steps, the IrO_x/TaTO catalysts demonstrated between 70 and 90% activity retention vs. 60% for the ATO-supported catalyst. The loss of the dopant was one-two orders of magnitude lower for Ta as compared to Sb, while the loss

Doi: 10.1595/205651321X16013966874707

of Sn was not affected. The Ir dissolution was found dependent on the Ta loading: the higher loading decreased Ir oxidation state contributing to its dissolution, while at lower loadings tantalum shell suppressed IrO_x nanoparticle detachment. This study (13) also demonstrates that the use of a support contributes to the enhanced Ir leaching, as compared to commercial IrO_2. As a result, although the activity of unsupported IrO_2 is significantly lower than that of the developed catalysts, its stability to dissolution contributes to high S-numbers (ratio of evolved oxygen to dissolved iridium)(21), such as, the S-number for IrO_2 was twice higher than that for selected IrO_x/TaTO catalysts at 1.6 V and similar at 1.5 V.(13) When hydrous IrO_x was supported on ATO, its S-number was also lower than the one for unsupported IrO_x, but the calcined supported samples demonstrated up to two orders of magnitude higher S-number as compared to IrO_2.(60)

When the above-mentioned (Section 3.2) surfactant-stabilized Ir nanodendrites (39 m^2/g area) were deposited on high-surface-area ATO (235 m^2/g), an initial overpotential of 260 mV at 10 mA/cm^2 at only 0.0102 mg_{Ir}/cm^2 loading (RDE, 0.05 M H_2SO_4) was observed while accelerated durability test showed a minor overpotential increase by 30 mV over 15 h compared to an abrupt increase for other tested catalysts at earlier times.(29) The specific current at 280 mV overpotential was reported at 70 A/g_{Ir} vs. 8 A/g_{Ir} for Ir black. In a PEM electrolyzer, the catalyst demonstrated the current density of 1.5 A/cm^2 at 1.8 V and 1 mg/cm^2 loading compared to 0.8 A/cm^2 for Ir black.

An atomically dispersed Ir on ITO with ultimate Ir dispersion was developed by grafting 0.86 wt.% Ir as an organometallic Ir complex followed by calcination in air at 400 °C.(65) The specific current of 156 A/g Ir was reached at 280 mV overpotential and 0.021 mg_{Ir}/cm^2 loading (0.1 M $HClO_4$). An overpotential of 350 ±20 mV was required to drive the 10 mA/cm^2 current at such low metal loadings over the course of 2 h; some Ir agglomeration was observed in the used catalyst and its consequences on the long-term performance requires further analysis.

From the catalyst synthesis viewpoint, one must be mindful that the support's chemical composition may change during the synthesis, affecting the electrochemical performance. For example, if Adams' method involving high-temperature calcination is used to produce IrO_2 on a carbide support, the support oxidation leads to the loss of conductivity (e.g., TaC lost its conductivity from 120 S/cm to 10^{-8} S/cm at such circumstances).(35) A similar carbide oxidation to a less-conductive oxide was reported for the Ir nanoparticle synthesis in the

Doi: 10.1595/205651321X16013966874707

presence of a support by a polyol method (heating in a reducing ethylene glycol with precipitating NaOH).(58) Moreover, Ir, Sn and In oxides may form mixed oxides; the lattice vacancies are thus produced upon Sn and In in situ dissolution, improving the initial activity but jeopardizing the durability (66) due to enhanced Ir dissolution.

5. Mixed metal oxides

Development of multimetallic Ir-containing catalysts has recently attracted considerable attention as a means of enhancing the OER catalyst performance, as had been proved beneficial for the catalyst development for fuel cells and alkaline water electrolysis. However, with Ir being the most corrosion resistant metal and still dissolving under the acidic OER conditions, any other metal would have an even higher dissolution rate. A rather popular combination of Ir and Ru features high activities due to the higher OER activity of Ru than that of Ir, but is not practical because of low corrosion resistance of Ru, which is also a scarce and expensive metal. The studies of the mixed oxide OER catalysts do typically address (and inevitably show) the dissolution of the catalyst components, but there is a lack of studies on the effect of the leached ions on the PEM system level. It is likely that the non-Ir cations may not only ion-exchange on Nafion changing its properties,(67) but may also travel to the cathode side and poison the Pt cathode as was shown for Ir.(42) Membrane degradation may also occur due to the attack of $HO^{\bullet}$ and other radicals, whose formation is catalyzed by transition metal cations. (46) For example, iron and copper ions were shown to dramatically enhance membrane degradation.(68)

Thus, a practical mixed oxide catalyst for an acidic OER application may be envisioned as one of the following composites (Fig. 6): (i) an IrO_x shell fully covering the core with an earth-abundant metal increasing the iridium dispersion; in this case, electrolyte contamination with the second metal may be delayed as compared to the mixed alloys until the iridium shell atoms leach exposing the core atoms; ii) Ir nanostructures produced by the preliminary removal of a sacrificial second component from a bimetallic composite, either by potential cycling or chemically. The selective leaching of the second component leads to surface restructuring,(69) porosity enhancement,(39) formation of lattice vacancies,(70) and ECSA increase.(71) Lattice vacancies formation via secondary metal leaching is a unique opportunity to modify the electrophilicity and Ir-O bond length leading to the enhanced OER activity as compared to IrO_x synthesized only from an Ir precursor. (70, 72) Some works

Doi: 10.1595/205651321X16013966874707

report, though, that Ir leaching from the composites may be even increased due to the created lattice vacancies, as compared to monometallic Ir catalysts.(39)

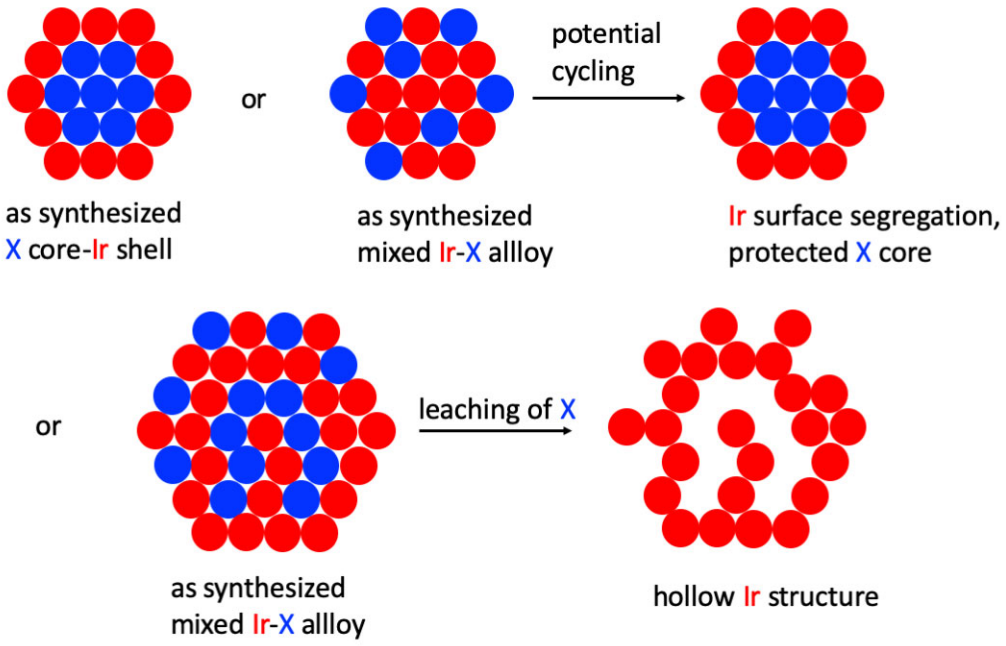

Figure 6. Mixed metal oxides for the acidic OER catalyst preparation.

Below, we provide some examples for such catalyst synthesis and performance. We note that the direct deposition methods, such as reactive sputtering and physical vapor deposition, are very frequently used for the mixed oxide studies, (39, 71–75) because they ensure structures with well-controlled composition and stoichiometry, thus, enabling the fundamental understanding of the composite's behavior. As this review does not cover the catalyst layer preparation methods, we only focus on the production of metal oxide powders or colloidal dispersions which were or could be mixed with the Nafion solution.

5.1. Core-shell bimetallic nanoparticles

Multimetallic composites can be synthesized using all the techniques applicable for monometallic catalyst synthesis (see Section 3) with the addition of the second precursor, with the fine tuning of the reaction conditions. Very often, both precursors are added together during the synthesis. Simultaneous reduction of different ions with different redox potentials

Doi: 10.1595/205651321X16013966874707

leads to the formation of either mixed alloy particles or core/shell nanoparticles.(76) For the core-shell synthesis, methods like ionic substitution (galvanic replacement) can be used (77) where a precursor of the second metal is deposited onto the metallic nanoparticles of the other metal based on the standard electrochemical potential (78), or a hydrogen-sacrificial method (79) where a core metal is hydrogenated, followed by the second ion reduction by the surface hydrides and shell formation. It is important to understand that thermodynamically unstable bimetallic structures can be synthesized (in terms of metal distribution) but how fast they rearrange into the thermodynamically stable composites (for example, where a metal with a lower cohesive energy segregates to the surface) depends on temperature, chemical and electrical environment. Metals can even change their location in situ depending on the catalyzed reaction or treatment conditions via so-called adsorbate-induced segregation.(80–82) Under the OER conditions, the restructuring may be expected to be an on-going process with transient equilibrium states due to the different rates of metal dissolution.

According to the Hume-Rothery substitution rule, in order to form a continuous solid solution, it is imperative that the difference between the atomic radii of the solvent and the solute not exceed 15% of each other and they should possess similar crystal structures. (83) One of the most common metals alloyed with Ir is Ru, but regardless of the efforts being made to inhibit Ru leaching, literature report continuous Ru dissolution, irrespective of methods of synthesis and structure of the mixed metals oxides. Ruban et al. reported a comprehensive table of surface segregation energies in transition-metal alloys, which can help predicting the final dealloyed structure of Ir composites.(84) In bimetallic alloys with Ir, metals such as Cu, Zr, Rh, Pd, Ag, Hf, Pt and Au would segregate to the surface, while Ir would surface-segregate from alloys with Ti, V, Cr, Mn, Fe, Co, Ni, Nb, Mo, Tc, Ru, Ta, W, Re, and Os.(84) Indeed, for example, in Ru-Ir alloys Ir formed a protective shell, offering an extended stability to Ru.(85)

Another example, conforming to the Ir surface segregation prediction, relates to the Ir-Ni composite. Bimetallic 7-nm $IrNi_{3.2}$ alloy nanoparticles were prepared by a simultaneous reduction of Ir and Ni precursors in the presence of a stabilizer.(70) The followed potential cycling from 0.05 to 1.5 V_{RHE} for 50 cycles resulted in partial Ni leaching, dealloying and oxidation with the formation of a metallic IrNi alloy(core)-IrO_x(shell) nanostructure. The IrO_x shells are doped with holes (originated from Ni leaching); they feature shorter Ir-O bonds and are more electrophilic than conventional iridium oxide, which affects the rate of O-O bond formation during OER and enhanced intrinsic activity per Ir site. A specific current of 676 A/g_{Ir}

Doi: 10.1595/205651321X16013966874707

was reported at 300 mV overpotential with 0.0102 mg_{Ir}/cm^2 loading, which is one of the highest in the above presented examples.(70) This example shows an extraordinary combination of increased Ir utilization due to its preferential location in the nanoparticle shell, as well as its beneficial electronic and thus catalytic activity modification upon dealloying.

5.2. Selective leaching of the sacrificial component (hard templating)

When a secondary metal in bimetallic composites with Ir is selectively removed, the process results in the formation of porous Ir nanostructures with high accessible active site density and/or modified IrO_x electronic and geometric properties, which cannot be achieved via a monometallic Ir catalyst synthesis. Some examples of a sacrificial metal are Ni,(14, 86) Co,(86) and Os.(39) Among different leaching methods, the most common are acid leaching (14) and potential cycling. (39, 71) For example, Ir was deposited on Ni nanowires via galvanic displacement, followed by the nanowires ("hard template") removal by acid leaching. (14) The residual composite with 90.5 wt.% Ir demonstrated a specific current of 1650 A/g_{Ir} at 0.0306 mg/cm^2 loading at 300 mV overpotential inn RDE in 0.1 M $HClO_4$. A parent mixed metal structure can be prepared as stabilized nanoparticles in a colloidal solution, such as an Ir-Os oxide.(39) The potential cycling resulted in dealloying and fast Os dissolution, leaving behind a nanoporous architecture of iridium metal core and IrO_x shell with an optimized stability and conductivity.(39) An important observation was that a high amount of Os-Ir bonds in the parent alloy led to the maximum Ir dissolution upon fast Os leaching.

This category features some of the most architecturally-sophisticated porous nanostructures, such as hollow nanocrystals synthesized via formation of a Ir-Co-Ni solid nanoparticles, followed by Co and Ni etching with Fe^{3+},(86) or double-layered nanoframes produced in a solution via reduction of Ni, Cu and two types of Ir precursors with different reduction kinetics followed by acid leaching.(87) Theoretically, this approach may produce highly porous connected Ir-only nanostructures, but its practical implementation is complicated by the nuances in the size and structure control, as well as secondary component complete leaching without the structure collapse.

It appears that the main achievement of the selective etching is not in the improvement of Ir surface area and dispersion, as the thus-synthesized catalysts do not feature areas above 100 m^2/g as compared with monometallic IrO_2 synthesized by Adams' method with 250

Doi: 10.1595/205651321X16013966874707

m^2/g.(31) Instead, the etching allows for modification of the IrO_x electronic structure and vacancies, affecting its OER activity and stability.

6. Conclusions

The fast-growing pool of published studies on the Ir-catalyzed acidic OER continually contributes to the mechanistic understanding of Ir activity and durability, the role of the second metal in alloys, and metal-support interactions. As a myriad of more or less sophisticated methods and structures emerges, one must keep in mind the method practicality, safety, ease, and scalability, and that it must use as little resources and produce as little waste as possible. This, most likely, precludes the use of surfactant-assisted routes of the wet catalyst synthesis and might jeopardize the stabilizer-free colloidal synthesis in vast amounts of organic solvents.

Despite the many advances on catalyst synthesis, and recently proposed metrics to assess catalyst activity and stability, such as the S-number and the activity-stability factor, a lack of consensus on the metrics used to report catalyst performance, as well as the electrochemical testing benchmarking procedures, make the comparison of different catalysts challenging. Activity studies reviewed for the fresh catalysts are not always accompanied by meaningful stability assessment, and high reported activities should be regarded with care, as the most active (hydrous) amorphous IrO_x is less stable than the less active crystalline IrO_2. With such considerations, it appears, to our subjective opinion, that Adams' fusion method (or other thermal methods) producing relatively stable rutile, deserve closer attention and further modifications. To take advantage of the enhanced activity of electrophilic oxygen sites, as follows from the multioxide studies, modification of the electrophilicity and Ir-O bond length via secondary metal leaching is a possible way to bridge the gap between the activity and stability. The use of supported may increase the stability of the calcined catalysts, however, the addition of dopants to improve electrical conductivity must be used with care.

One must keep in mind that the catalyst layer fabrication can have a tremendous effect on the activity observed in a real electrode. The ionomer-to-catalyst ratio, particle size, the use of a support, catalyst-ionomer-solvent interactions in the dispersion, and deposition technique, can have a significant impact on the electrode electrochemical surface area, ion and electron conductivity, and its ability to transport reactant and by-products in and out of the cell. Gas-phase catalyst synthesis and deposition methods, e.g., (8), which were not

Doi: 10.1595/205651321X16013966874707

reviewed here, may provide a promising alternative to the wet-chemistry techniques. Moving forward, not only the catalyst synthesis, but also development of common characterization techniques and metrics to assess activity and stability in RDE, and optimal electrode fabrication methods must become paramount in our collective effort to develop the most efficient OER catalyst, and OER electrode.

Acknowledgements

As a part of the University of Alberta's Future Energy Systems research initiative, this research was made possible thanks to funding from the Canada First Research Excellence Fund (https://futureenergysystems.ca; Grant No. T06-P04).

The Authors

Himanshi Dhawan completed her Bachelor's in Technology in Chemical Engineering from India. In January 2019, she started her Ph.D. at the University of Alberta, Edmonton, Canada where she is currently working on developing iridium based electrocatalysts for oxygen evolution reaction in acidic media.

Marc Secanell is a Professor in the Department of Mechanical Engineering at the University of Alberta. His research focuses on multi-scale numerical modeling of electrochemical system, such as the development of the open-source fuel cell simulation toolbox (openFCST, www.openfcst.org), and the experimental fabrication, characterization and testing of polymer electrolyte fuel cell and electrolyzer electrodes.

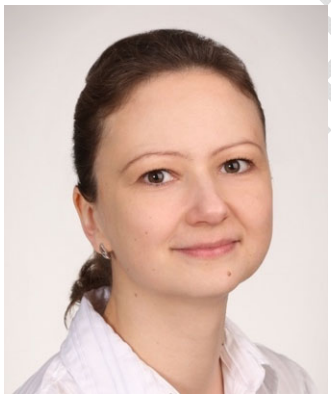

Natalia Semagina is a Professor in the Department of Chemical and Materials Engineering at the University of Alberta. Her research focuses on experimental heterogeneous catalysis, controlled synthesis of mono- and bimetallic nanoparticles, and elucidation of a catalyst's structure-activity relationship in a variety of applications.

References

1. C. Vogt, M. Monai, G. J. Kramer and B. M. Weckhuysen, *Nat. Catal.*, 2019, **2**, (3), 188 LINK https://doi.org/10.1038/s41929-019-0244-4
2. S. A. Grigoriev, V. N. Fateev, D. G. Bessarabov and P. Millet, *Int. J. Hydrogen Energy*, 2020, (xxxx), LINK https://doi.org/10.1016/j.ijhydene.2020.03.109
3. K. A. Lewinski, D. van der Vliet and S. M. Luopa, *ECS Trans.*, 2015, **69**, (17), 893 LINK https://doi.org/10.1149/06917.0893ecst
4. J. Kibsgaard and I. Chorkendorff, *Nat. Energy*, 2019, **4**, (6), 430 LINK https://doi.org/10.1038/s41560-019-0407-1
5. 'The Future of Hydrogen. IEA Technology Report', , 2019 LINK https://doi.org/https://www.iea.org/reports/the-future-of-hydrogen
6. C. Wang, F. Lan, Z. He, X. Xie, Y. Zhao, H. Hou, L. Guo, V. Murugadoss, H. Liu, Q. Shao, Q. Gao, T. Ding, R. Wei and Z. Guo, *ChemSusChem*, 2019, **12**, (8), 1576 LINK https://doi.org/10.1002/cssc.201802873
7. H. Jang and J. Lee, *J. Energy Chem.*, 2020, **46**, 152 LINK https://doi.org/10.1016/j.jechem.2019.10.026
8. H. Yu, N. Danilovic, Y. Wang, W. Willis, A. Poozhikunnath, L. Bonville, C. Capuano, K. Ayers and R. Maric, *Appl. Catal. B Environ.*, 2018, **239**, (July), 133 LINK https://doi.org/10.1016/j.apcatb.2018.07.064
9. J. M. Roller, M. Josefina Arellano-Jiménez, R. Jain, H. Yu, C. Barry Carter and R. Maric, *J. Electrochem. Soc.*, 2013, **160**, (6), F716 LINK https://doi.org/10.1149/2.121306jes
10. P. Lettenmeier, J. Majchel, L. Wang, V. A. Saveleva, S. Zafeiratos, E. R. Savinova, J. J. Gallet, F. Bournel, A. S. Gago and K. A. Friedrich, *Chem. Sci.*, 2018, **9**, (14), 3570 LINK https://doi.org/10.1039/c8sc00555a
11. F. Bizzotto, J. Quinson, A. Zana, J. J. K. Kirkensgaard, A. Dworzak, M. Oezaslan and M. Arenz, *Catal. Sci. Technol.*, 2019, **9**, (22), 6345 LINK https://doi.org/10.1039/c9cy01728c
12. J. Chen, P. Cui, G. Zhao, K. Rui, M. Lao, Y. Chen, X. Zheng, Y. Jiang, H. Pan, S. X. Dou and W. Sun, *Angew. Chemie - Int. Ed.*, 2019, **58**, (36), 12540 LINK https://doi.org/10.1002/anie.201907017
13. S. Abbou, R. Chattot, V. Martin, F. Claudel, L. Solà-Hernandez, C. Beauger, L. Dubau and F. Maillard, *ACS Catal.*, 2020, **10**, (13), 7283 LINK https://doi.org/10.1021/acscatal.0c01084
14. S. M. Alia, S. Shulda, C. Ngo, S. Pylypenko and B. S. Pivovar, *ACS Catal.*, 2018, **8**, (3),

2111 LINK https://doi.org/10.1021/acscatal.7b03787

15. M. Bernt, A. Siebel and H. A. Gasteiger, *J. Electrochem. Soc.*, 2018, **165**, (5), F305 LINK https://doi.org/10.1149/2.0641805jes
16. M. Bernt, A. Hartig-Weiß, M. F. Tovini, H. A. El-Sayed, C. Schramm, J. Schröter, C. Gebauer and H. A. Gasteiger, *Chemie-Ingenieur-Technik*, 2020, **92**, (1–2), 31 LINK https://doi.org/10.1002/cite.201900101
17. M. Tahir, L. Pan, F. Idrees, X. Zhang, L. Wang, J. J. Zou and Z. L. Wang, *Nano Energy*, 2017, **37**, (May), 136 LINK https://doi.org/10.1016/j.nanoen.2017.05.022
18. T. Reier, H. N. Nong, D. Teschner, R. Schlögl and P. Strasser, *Adv. Energy Mater.*, 2017, **7**, (1), LINK https://doi.org/10.1002/aenm.201601275
19. T. Schuler, T. Kimura, T. J. Schmidt and F. N. Büchi, *Energy Environ. Sci.*, 2020, (2), 2153 LINK https://doi.org/10.1039/d0ee00673d
20. V. A. Saveleva, L. Wang, D. Teschner, T. Jones, A. S. Gago, K. A. Friedrich, S. Zafeiratos, R. Schlögl and E. R. Savinova, *J. Phys. Chem. Lett.*, 2018, **9**, (11), 3154 LINK https://doi.org/10.1021/acs.jpclett.8b00810
21. S. Geiger, O. Kasian, M. Ledendecker, E. Pizzutilo, A. M. Mingers, W. T. Fu, O. Diaz-Morales, Z. Li, T. Oellers, L. Fruchter, A. Ludwig, K. J. J. Mayrhofer, M. T. M. Koper and S. Cherevko, *Nat. Catal.*, 2018, **1**, (7), 508 LINK https://doi.org/10.1038/s41929-018-0085-6
22. A. Grimaud, A. Demortiere, M. Saubanere, W. Dachraoui, M. Duchamp, M. L. Doublet and J. M. Tarascon, *Nat. Energy*, 2017, **2**, (1), LINK https://doi.org/10.1038/nenergy.2016.189
23. V. Pfeifer, T. E. Jones, J. J. Velasco Vélez, C. Massué, M. T. Greiner, R. Arrigo, D. Teschner, F. Girgsdies, M. Scherzer, J. Allan, M. Hashagen, G. Weinberg, S. Piccinin, M. Hävecker, A. Knop-Gericke and R. Schlögl, *Phys. Chem. Chem. Phys.*, 2016, **18**, (4), 2292 LINK https://doi.org/10.1039/c5cp06997a
24. O. Kasian, S. Geiger, T. Li, J. P. Grote, K. Schweinar, S. Zhang, C. Scheu, D. Raabe, S. Cherevko, B. Gault and K. J. J. Mayrhofer, *Energy Environ. Sci.*, 2019, **12**, (12), 3548 LINK https://doi.org/10.1039/c9ee01872g
25. X. Tan, J. Shen, N. Semagina and M. Secanell, *J. Catal.*, 2019, **371**, 57 LINK https://doi.org/10.1016/j.jcat.2019.01.018
26. T. Li, O. Kasian, S. Cherevko, S. Zhang, S. Geiger, C. Scheu, P. Felfer, D. Raabe, B. Gault and K. J. J. Mayrhofer, *Nat. Catal.*, 2018, **1**, (4), 300 LINK https://doi.org/10.1038/s41929-018-0043-3
27. O. Kasian, J. P. Grote, S. Geiger, S. Cherevko and K. J. J. Mayrhofer, *Angew. Chemie* -

Int. Ed., 2018, **57**, (9), 2488 LINK https://doi.org/10.1002/anie.201709652

28. S. Geiger, O. Kasian, B. R. Shrestha, A. M. Mingers, K. J. J. Mayrhofer and S. Cherevko, *J. Electrochem. Soc.*, 2016, **163**, (11), F3132 LINK https://doi.org/10.1149/2.0181611jes
29. H. S. Oh, H. N. Nong, T. Reier, M. Gliech and P. Strasser, *Chem. Sci.*, 2015, **6**, (6), 3321 LINK https://doi.org/10.1039/c5sc00518c
30. B. J. Kip, J. Van Grondelle, J. H. A. Martens and R. Prins, *Appl. Catal.*, 1986, **26**, (C), 353 LINK https://doi.org/10.1016/S0166-9834(00)82564-6
31. M. Povia, D. F. Abbott, J. Herranz, A. Heinritz, D. Lebedev, B. J. Kim, E. Fabbri, A. Patru, J. Kohlbrecher, R. Schäublin, M. Nachtegaal, C. Copéret and T. J. Schmidt, *Energy Environ. Sci.*, 2019, **12**, (10), 3038 LINK https://doi.org/10.1039/c9ee01018a
32. E. Özer, C. Spöri, T. Reier and P. Strasser, *ChemCatChem*, 2017, **9**, (4), 597 LINK https://doi.org/10.1002/cctc.201600423
33. S. Cherevko, S. Geiger, O. Kasian, A. Mingers and K. J. J. Mayrhofer, *J. Electroanal. Chem.*, 2016, **774**, 102 LINK https://doi.org/10.1016/j.jelechem.2016.05.015
34. T. Reier, M. Oezaslan and P. Strasser, *ACS Catal.*, 2012, **2**, (8), 1765 LINK https://doi.org/10.1021/cs3003098
35. A. V. Nikiforov, C. B. Prag, J. Polonský, I. M. Petrushina, E. Christensen and N. J. Bjerrum, *ECS Trans.*, 2012, **41(42)**, 115 LINK https://doi.org/10.1149/1.4718004
36. M. Bernt and H. A. Gasteiger, *J. Electrochem. Soc.*, 2016, **163**, (11), F3179 LINK https://doi.org/10.1149/2.0231611jes
37. M. Mandal, M. Moore and M. Secanell, *ECS Trans.*, 2019, **92**, (8), 757 LINK https://doi.org/10.1149/09208.0757ecst
38. T. Schuler, J. M. Ciccone, B. Krentscher, F. Marone, C. Peter, T. J. Schmidt and F. N. Büchi, *Adv. Energy Mater.*, 2020, **10**, (2), 1 LINK https://doi.org/10.1002/aenm.201903216
39. Y. T. Kim, P. P. Lopes, S. A. Park, A. Y. Lee, J. Lim, H. Lee, S. Back, Y. Jung, N. Danilovic, V. Stamenkovic, J. Erlebacher, J. Snyder and N. M. Markovic, *Nat. Commun.*, 2017, **8**, (1), 1 LINK https://doi.org/10.1038/s41467-017-01734-7
40. Q. Feng, X. Z. Yuan, G. Liu, B. Wei, Z. Zhang, H. Li and H. Wang, *J. Power Sources*, 2017, **366**, 33 LINK https://doi.org/10.1016/j.jpowsour.2017.09.006
41. U. Babic, M. Tarik, T. J. Schmidt and L. Gubler, *J. Power Sources*, 2020, **451**, (January), 227778 LINK https://doi.org/10.1016/j.jpowsour.2020.227778
42. H. Yu, L. Bonville, J. Jankovic and R. Maric, *Appl. Catal. B Environ.*, 2020, **260**, (July 2019), 118194 LINK https://doi.org/10.1016/j.apcatb.2019.118194

43. S. Martens, L. Asen, G. Ercolano, F. Dionigi, C. Zalitis, A. Hawkins, A. Martinez Bonastre, L. Seidl, A. C. Knoll, J. Sharman, P. Strasser, D. Jones and O. Schneider, *J. Power Sources*, 2018, **392**, (April), 274 LINK https://doi.org/10.1016/j.jpowsour.2018.04.084
44. S. Geiger, O. Kasian, A. M. Mingers, S. S. Nicley, K. Haenen, K. J. J. Mayrhofer and S. Cherevko, *ChemSusChem*, 2017, **10**, (21), 4140 LINK https://doi.org/10.1002/cssc.201701523
45. F. M. Sapountzi, S. C. Divane, E. I. Papaioannou, S. Souentie and C. G. Vayenas, *J. Electroanal. Chem.*, 2011, **662**, (1), 116 LINK https://doi.org/10.1016/j.jelechem.2011.04.005
46. U. Babic, M. Suermann, F. N. Büchi, L. Gubler and T. J. Schmidt, *J. Electrochem. Soc.*, 2017, **164**, (4), F387 LINK https://doi.org/10.1149/2.1441704jes
47. C. C. L. McCrory, S. Jung, J. C. Peters and T. F. Jaramillo, *J. Am. Chem. Soc.*, 2013, **135**, (45), 16977 LINK https://doi.org/10.1021/ja407115p
48. I. Spanos, A. A. Auer, S. Neugebauer, X. Deng, H. Tüysüz and R. Schlögl, *ACS Catal.*, 2017, **7**, (6), 3768 LINK https://doi.org/10.1021/acscatal.7b00632
49. C. Spöri, J. T. H. Kwan, A. Bonakdarpour, D. P. Wilkinson and P. Strasser, *Angew. Chemie - Int. Ed.*, 2017, **56**, (22), 5994 LINK https://doi.org/10.1002/anie.201608601
50. L.B.H., *Platin. Met. Rev.*, 1962, **6**, (4), 150 LINK http://www.platinummetalsreview.com/pdf/pmr-v6-i4-150-152.pdf
51. R. Adams and R. L. Shriner, *J. Am. Chem. Soc.*, 1923, **45**, (9), 2171 LINK https://doi.org/10.1021/ja01662a022
52. E. Rasten, G. Hagen and R. Tunold, *Electrochim. Acta*, 2003, **48**, (25–26), 3945 LINK https://doi.org/10.1016/j.electacta.2003.04.001
53. D. F. Abbott, D. Lebedev, K. Waltar, M. Povia, M. Nachtegaal, E. Fabbri, C. Copéret and T. J. Schmidt, *Chem. Mater.*, 2016, **28**, (18), 6591 LINK https://doi.org/10.1021/acs.chemmater.6b02625
54. J. Lim, D. Park, S. S. Jeon, C. W. Roh, J. Choi, D. Yoon, M. Park, H. Jung and H. Lee, *Adv. Funct. Mater.*, 2018, **28**, (4), 1 LINK https://doi.org/10.1002/adfm.201704796
55. N. Semagina and L. Kiwi-Minsker, 'Recent Advances in the Liquid-Phase Synthesis of Metal Nanostructures with Controlled Shape and Size for Catalysis', 'Catal. Rev. - Sci. Eng.', Vol. 51, 2009 LINK https://doi.org/10.1080/01614940802480379
56. P. T. Witte, P. H. Berben, S. Boland, E. H. Boymans, D. Vogt, J. W. Geus and J. G. Donkervoort, *Top. Catal.*, 2012, **55**, (7–10), 505 LINK https://doi.org/10.1007/s11244-012-9818-y

57. J. Quinson, S. Neumann, T. Wannmacher, L. Kacenauskaite, M. Inaba, J. Bucher, F. Bizzotto, S. B. Simonsen, L. Theil Kuhn, D. Bujak, A. Zana, M. Arenz and S. Kunz, *Angew. Chemie - Int. Ed.*, 2018, **57**, (38), 12338 LINK https://doi.org/10.1002/anie.201807450
58. F. Karimi and B. A. Peppley, *Electrochim. Acta*, 2017, **246**, 654 LINK https://doi.org/10.1016/j.electacta.2017.06.048
59. S. Geiger, O. Kasian, A. M. Mingers, K. J. J. Mayrhofer and S. Cherevko, *Sci. Rep.*, 2017, **7**, (1), 3 LINK https://doi.org/10.1038/s41598-017-04079-9
60. G. C. da Silva, S. I. Venturini, S. Zhang, M. Löffler, C. Scheu, K. J. J. Mayrhofer, E. A. Ticianelli and S. Cherevko, *ChemElectroChem*, 2020, **7**, (10), 2330 LINK https://doi.org/10.1002/celc.202000391
61. H. S. Oh, H. N. Nong, T. Reier, A. Bergmann, M. Gliech, J. Ferreira De Araújo, E. Willinger, R. Schlögl, D. Teschner and P. Strasser, *J. Am. Chem. Soc.*, 2016, **138**, (38), 12552 LINK https://doi.org/10.1021/jacs.6b07199
62. H. S. Oh, H. N. Nong and P. Strasser, *Adv. Funct. Mater.*, 2015, **25**, (7), 1074 LINK https://doi.org/10.1002/adfm.201401919
63. C. Massué, V. Pfeifer, X. Huang, J. Noack, A. Tarasov, S. Cap and R. Schlögl, *ChemSusChem*, 2017, **10**, (9), 1943 LINK https://doi.org/10.1002/cssc.201601817
64. D. Lebedev and C. Copéret, *ACS Appl. Energy Mater.*, 2019, **2**, (1), 196 LINK https://doi.org/10.1021/acsaem.8b01724
65. D. Lebedev, R. E. Ezhov, J. Heras-Domingo, A. C. Vives, N. Kaeffer, M. Willinger, X. Solans-Monfort, H. Xing, Y. Pushkar and C. Copéret, *ChemRxiv*, 2020, 10.26434/chemrxiv.11852643.v1 LINK https://doi.org/10.26434/chemrxiv.11852643.v1
66. M. Ledendecker, S. Geiger, K. Hengge, J. Lim, S. Cherevko, A. M. Mingers, D. Göhl, G. V. Fortunato, D. Jalalpoor, F. Schüth, C. Scheu and K. J. J. Mayrhofer, *Nano Res.*, 2019, **12**, (9), 2275 LINK https://doi.org/10.1007/s12274-019-2383-y
67. S. Shi, A. Z. Weber and A. Kusoglu, *Electrochim. Acta*, 2016, **220**, 517 LINK https://doi.org/10.1016/j.electacta.2016.10.096
68. T. Kinumoto, M. Inaba, Y. Nakayama, K. Ogata, R. Umebayashi, A. Tasaka, Y. Iriyama, T. Abe and Z. Ogumi, *J. Power Sources*, 2006, **158**, (2 SPEC. ISS.), 1222 LINK https://doi.org/10.1016/j.jpowsour.2005.10.043
69. C. Spöri, P. Briois, H. N. Nong, T. Reier, A. Billard, S. Kühl, D. Teschner and P. Strasser, *ACS Catal.*, 2019, **9**, (8), 6653 LINK https://doi.org/10.1021/acscatal.9b00648
70. H. N. Nong, T. Reier, H. S. Oh, M. Gliech, P. Paciok, T. H. T. Vu, D. Teschner, M.

Heggen, V. Petkov, R. Schlögl, T. Jones and P. Strasser, *Nat. Catal.*, 2018, **1**, (11), 841 LINK https://doi.org/10.1038/s41929-018-0153-y

71. O. Kasian, S. Geiger, M. Schalenbach, A. M. Mingers, A. Savan, A. Ludwig, S. Cherevko and K. J. J. Mayrhofer, *Electrocatalysis*, 2018, **9**, (2), 139 LINK https://doi.org/10.1007/s12678-017-0394-6
72. L. C. Seitz, C. F. Dickens, K. Nishio, Y. Hikita, J. Montoya, A. Doyle, C. Kirk, A. Vojvodic, H. Y. Hwang, J. K. Norskov and T. F. Jaramillo, *Science (80-.).*, 2016, **353**, (6303), 1011
73. A. W. Jensen, G. W. Sievers, K. D. Jensen, J. Quinson, J. A. Arminio-Ravelo, V. Brüser, M. Arenz and M. Escudero-Escribano, *J. Mater. Chem. A*, 2020, **8**, (3), 1066 LINK https://doi.org/10.1039/c9ta12796h
74. A. L. Strickler, R. A. Flores, L. A. King, J. K. Nørskov, M. Bajdich and T. F. Jaramillo, *ACS Appl. Mater. Interfaces*, 2019, **11**, (37), 34059 LINK https://doi.org/10.1021/acsami.9b13697
75. O. Kasian, S. Geiger, P. Stock, G. Polymeros, B. Breitbach, A. Savan, A. Ludwig, S. Cherevko and K. J. J. Mayrhofer, *J. Electrochem. Soc.*, 2016, **163**, (11), F3099 LINK https://doi.org/10.1149/2.0131611jes
76. N. Toshima, *Pure Appl. Chem.*, 2000, **72**, (1–2), 317 LINK https://doi.org/10.1351/pac200072010317
77. C. Wang, Y. Sui, G. Xiao, X. Yang, Y. Wei, G. Zou and B. Zou, *J. Mater. Chem. A*, 2015, **3**, (39), 19669 LINK https://doi.org/10.1039/c5ta05384f
78. B. Coq and F. Figueras, *J. Mol. Catal. A Chem.*, 2001, **173**, (1–2), 117 LINK https://doi.org/10.1016/S1381-1169(01)00148-0
79. H. Ziaei-Azad and N. Semagina, *ChemCatChem*, 2014, **6**, (3), 885 LINK https://doi.org/10.1002/cctc.201300844
80. F. Tao, M. E. Grass, Y. Zhang, D. R. Butcher, J. R. Renzas, Z. Liu, J. Y. Chung, B. S. Mun, M. Salmeron and G. A. Somorjai, *Science (80-.).*, 2008, **322**, (November), 932
81. X. Liu, A. Wang, L. Li, T. Zhang, C. Y. Mou and J. F. Lee, *J. Catal.*, 2011, **278**, (2), 288 LINK https://doi.org/10.1016/j.jcat.2010.12.016
82. K. J. J. Mayrhofer, V. Juhart, K. Hartl, M. Hanzlik and M. Arenz, *Angew. Chemie - Int. Ed.*, 2009, **48**, (19), 3529 LINK https://doi.org/10.1002/anie.200806209
83. C. Felix, T. Maiyalagan, S. Pasupathi, B. Bladergroen and V. Linkov, *Int. J. Electrochem. Sci.*, 2012, **7**, (12), 12064
84. A. V. Ruban, H. L. Skriver and J. K. Nørskov, *Phys. Rev. B - Condens. Matter Mater. Phys.*, 1999, **59**, (24), 15990 LINK https://doi.org/10.1103/PhysRevB.59.15990

85. N. Danilovic, R. Subbaraman, K. C. Chang, S. H. Chang, Y. Kang, J. Snyder, A. P. Paulikas, D. Strmcnik, Y. T. Kim, D. Myers, V. R. Stamenkovic and N. M. Markovic, *Angew. Chemie - Int. Ed.*, 2014, **53**, (51), 14016 LINK https://doi.org/10.1002/anie.201406455

86. J. Feng, F. Lv, W. Zhang, P. Li, K. Wang, C. Yang, B. Wang, Y. Yang, J. Zhou, F. Lin, G. C. Wang and S. Guo, *Adv. Mater.*, 2017, **29**, (47), 1 LINK https://doi.org/10.1002/adma.201703798

87. J. Park, Y. J. Sa, H. Baik, T. Kwon, S. H. Joo and K. Lee, *ACS Nano*, 2017, **11**, (6), 5500 LINK https://doi.org/10.1021/acsnano.7b00233